Computational Modeling of Piezochromism in Molecular Crystals

Xibo Feng,[1, a)] Axel D. Becke,[1, b)] and Erin R. Johnson*[1, c)]
Department of Chemistry, Dalhousie University, 6274 Coburg Road, P.O. Box 15000, Halifax, Nova Scotia B3H 4R2, Canada

(Dated: 19 May 2020)

Piezochromic materials, whose luminescence responds to external pressure, have recently garnered much experimental attention. Computational modeling of piezochromism is of high theoretical interest, yet currently lacking. Herein, we present a computational effort to predict the piezochromism for a selection of molecular crystals. The current methodology employs a combination of dispersion-corrected solid-state and gas-phase density-functional theory (DFT), and Becke's virial exciton model. Our study finds that piezochromism is primarily driven by the modification of intermolecular interactions within the molecular crystal and can be understood from the perspectives of changing polarizability or band gaps upon the application of mechanical pressure.

I. INTRODUCTION

Piezochromism[1] refers to changes in the photoluminescence (PL) wavelength and/or intensity of certain molecular crystals in response to the external stimulus of mechanical pressure (grinding or hydraulic pressure). Molecular crystals that display piezochromism have attracted considerable research attention, due to their potential applications in fields such as mechano-sensors,[2,3] memory devices,[4,5] and optoelectronics.[6,7] The potential utility of many piezochromic materials also lies in the fact they concurrently possess aggregation-induced emission[8,9] (AIE), meaning that their PL is significantly enhanced in the crystalline form relative to a dilute solution. It has been hypothesized that piezochromic behaviors could be induced when the inter- or intra-molecular environment within the crystal is modulated through the change in the crystal packing mode, or simply spatial constriction, when external pressure is applied.[10–12]

Computational investigation of piezochromism in molecular crystals is theoretically intriguing, as it represents a challenging case where the interplay of multiple inter- and intramolecular factors might drive the modification of the electronic structure in the solid state, which is manifested by shifts in the crystals' luminescent properties. Despite much experimental effort to synthesize and characterize a variety of novel molecular crystals showing significant piezochromism,[10–16] theoretical modeling and rationalization of this phenomenon is currently limited.[17] We suspect that this is primarily due to complications in applying the popular time-dependent density-functional theory (TD-DFT[18,19]) method to periodic solids.

Traditionally, TD-DFT would be used as the QM component in the QM/MM[20] (quantum mechanics/molecular mechanics) embedding scheme, where a cluster surrounding the excited molecule is extracted from the crystal lattice as the system of interest.[17] One problem with the QM/MM scheme is the lack of Pauli repulsion between the QM and MM subsystems, which leads to the unphysical penetration of the QM-electron density into the MM subsystem.[21] The QM/MM scheme is also found to artificially accumulate QM-electronic charge at the QM/MM boundary when there exists an extensive H bond network.[22] In the context of modeling molecular crystals under pressure, these issues with the conventional QM(TD-DFT)/MM scheme are particularly undesirable, as minute changes in the intermolecular interactions within the lattice could very well be the driving factor of piezochromism. As an alternative to QM/MM, applying full TD-DFT to model the PL properties of bulk molecular crystals has only started to be explored[23–25], with recent advances[25,26] in the implementation of periodic-boundary TD-DFT in planewave/pseudopotential computational codes.

In this work, we first propose a novel computational scheme to model the photoexcitation/PL of molecular crystals. The current framework combines periodic-boundary and finite-molecule calculations using time-independent DFT. We then assess the ability of the proposed method to predict the known piezochromic behaviors of a selection of molecular crystals. From our results, we demonstrate that piezochromism in molecular crystals is predominantly driven by the the pressure modulation of the intermolecular interactions within the lattice. Finally, in order to rationalize the observed piezochromic PL wavelength shifts in molecular crystals, we investigate the changes in the crystal band gap and the molecular polarizability under applied pressure, which offer insights into the underlying mechanism of piezochromism from a solid-state and a molecular perspective, respectively.

Figure 1 shows the molecular structures of the three investigated molecular crystals. Organic chromophores **1**,[28] **2**,[29] and **3**[30] have been previously synthesized and crystallized. These crystals' experimentally-observed PL properties and piezochromic behaviors are summarized in Table I. Note that all three molecular crystals display a gradual red shift in the PL maximum wavelength under increasing isotropic hydraulic pressure. Such a red shift appears to be generally observed in the experimental literature. For the investigated crystals, this red shift is also reversible, *i.e.* the original PL maximum wavelength measured at ambient pressure is restored once the applied hydraulic pressure is removed.

[a)]Electronic mail: frederick.hillsfeng@dal.ca
[b)]Electronic mail: axel.becke@dal.ca
[c)]Electronic mail: erin.johnson@dal.ca; http://schooner.chem.dal.ca

FIG. 1: Molecular structures of the investigated piezochromic crystals, with their Cambridge Crystallographic Data Centre[27] (CCDC) identifiers included in parentheses. **1**: Tetrathiazolylthiophene, **2**: boron diketonate, **3**: 2,7-diaryl-[1,2,4]triazolo[1,5-a]pyrimidine (2,7-diaryl-TAP). For **1**, two crystal structures were reported, one measured under ambient pressure (FIFGUY01), and the other (FIFGUY02) under 2.8 GPa of isotropic hydraulic pressure.[28]

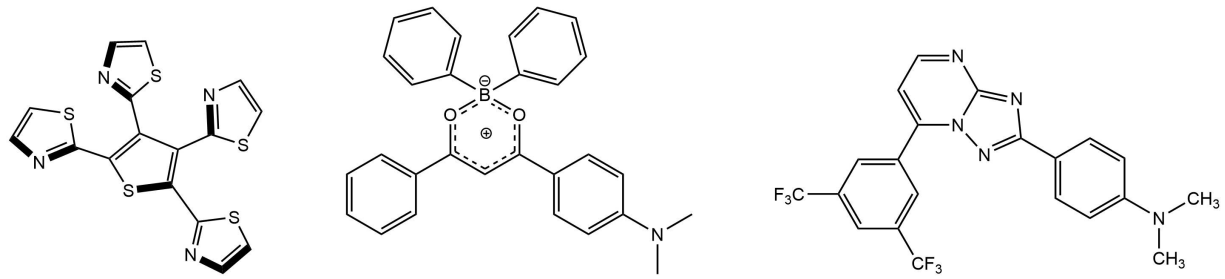

1 (FIFGUY01, FIFGUY02) **2** (XAPLUY) **3** (IXICUP)

TABLE I: Experimental PL properties and piezochromism of the investigated molecular crystals. $\lambda_{\max}^{\mathrm{emi}}$: emission maximum wavelength; ΔE^{emi}: emission energy.

Species	Ambient pressure		Highest pressure			Max. PL	Piezochromism	Ref.
	$\lambda_{\max}^{\mathrm{emi}}$ (nm)	ΔE^{emi} (eV)	$P_{\max}$ (GPa)	$\lambda_{\max}^{\mathrm{emi}}$ (nm)	ΔE^{emi} (eV)	shift (eV)	type	
1	556	2.23	3.20	609	2.04	0.19	Reversible red shift	28
2	585	2.14	5.77	660	1.88	0.26	Reversible red shift	29
3	524	2.37	14.5	676	1.83	0.53	Reversible red shift	30

II. COMPUTATIONAL METHODS

We employ a multi-step approach in this work involving standard density-functional theory (DFT) calculations on the target molecular crystals and on excised gas-phase molecular moieties. The crystals are modeled with the plane-wave formalism and projector augmented-wave[31] (PAW) atomic datasets. Computations are performed for the ground state (S_0) and the first excited triplet state (T_1), the latter using constrained magnetization to localize the excitation. A correction is then applied to the T_1 energy to obtain the first singlet (S_1) excited-state energy from gas-phase excised molecular calculations. The correction, or S_1-T_1 gap, is based on the virial exciton model of Becke[32] and the assumption that the excitation is localized on molecular sites in the crystal.

The S_1-T_1 gap is represented by the two-electron H_{12} integral (denoted as K_{if} in Ref. 32) and computed as the exchange integral involving the two singly occupied frontier orbitals of the molecular T_1 state:

$$H_{12} = \left\langle \phi_a(1)\phi_b(2) \left| \frac{1}{r_{12}} \right| \phi_a(2)\phi_b(1) \right\rangle. \qquad (1)$$

The virial exciton model has the advantage of computational simplicity, while also eliminating errors seen with TD-DFT for charge-transfer excitations.[33] It is assumed that the total electron densities in the T_1 and S_1 states are very similarly affected by the surrounding crystalline environment, so that the H_{12} value calculated in the gas phase for an extracted molecular moiety can be used to approximate the S_1-T_1 energy gap of the molecular crystal. Thus, the singlet exicitation energy in the crystal can be approximated as

$$\Delta E_{0\mathrm{S}}^{\mathrm{cryst}} = \Delta E_{0\mathrm{T}}^{\mathrm{cryst}} + H_{12}^{\mathrm{mol}}, \qquad (2)$$

where $\Delta E_{0\mathrm{T}}^{\mathrm{cryst}}$ is computed from periodic-boundary DFT and H_{12}^{mol} from finite-molecule calculations.

The virial exciton model itself also relies on the assumption that the T_1 and S_1 states have similar densities in the computation of the singlet-triplet splitting, H_{12}.[32] This assumption is based on the fact that the T_1 and S_1 states have identical orbital occupations, differing only in the spin of one electron, and is supported by the success of the model. One would expect the largest singlet-triplet density differences to occur for the smallest systems. The error introduced for the helium $1s2s$ singlet-triplet splitting is 0.20 eV,[32] and much smaller errors are expected for large organic molecules. Additionally, following our previous work,[34] the effect of excitation on the dispersion component of the lattice energy may be determined using the critic2 program.[35] The computed dispersion coefficients for a single ground-state molecule within the crystal lattice are replaced with the corresponding values for the T_1 or S_1 state, and the resulting intermolecular dispersion energy evaluated. The molecular excited-state densities were obtained from SCF calculations for T_1 and from TD-DFT for S_1, and the dispersion coefficients evaluated using the postg program.[36] For the three compounds considered here, the T_1 state experiences slightly greater dispersion interactions within the crystal; however, the lattice-energy differences are extremely small (*viz.* 0.02-0.10 kcal/mol). This supports our assumption that the S_1 and T_1 states will experience sufficiently similar intermolecular interactions with the

surrounding crystal lattice.

FIG. 2: The computational scheme employed in this work.

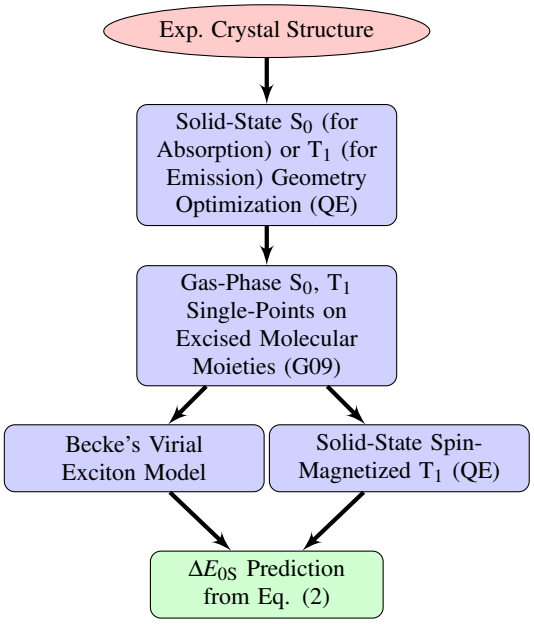

Figure 2 sketches the overall computational framework. We first optimized the S_0 geometries of the experimentally reported crystal structures, taken from the CCDC.[27] After the initial S_0 geometry optimizations, the crystal lattices were cut into (symmetry equivalent) molecular moieties using the critic2 program.[35] One single molecule was chosen, upon which single-point gas-phase calculations on the S_0 and T_1 (restricted open-shell, RO) states were performed. The resulting T_1 frontier orbitals were used to calculate the H_{12} integral. The initial spin-density biases used in the spin-magnetized calculation on the T_1 state in the crystal were then assigned based on the gas-phase RO spin-densities. To acquire the absorption energy, a single-point spin-magnetized T_1 calculation sufficed. For emission, spin-magnetized T_1 geometry optimization was performed, and the H_{12} integral was calculated again for the molecular moiety excised from the T_1-optimized crystal lattice.

All calculations on the molecular crystals were performed with the B86bPBE functional,[37,38] in conjunction with the exchange-hole dipole moment (XDM) model[39–41] dispersion correction. The Quantum ESPRESSO[42] (QE) package was used for these solid-state calculations. The "press" keyword was used to designate the isotropic pressure applied to the crystal lattice. For all QE calculations, the well-converged $2\times2\times2$ Monkhorst-Pack[43] k-point mesh and planewave cutoff values of 800 and 80 Ry for the wavefunction and density, respectively, were used. All PAW datasets were generated via the "atomic" code by Dal Corso.[44] Gas-phase calculations on the molecular moieties were performed for the S_0 and restricted open-shell T_1 states with the B3LYP[45] (for **1** and **2**) and the BHandHLYP[46] (for **3**, due to B3LYP's failure in RO convergence) functionals, using the Gaussian 09 (G09) package.[47] Molecular polarizabilities were calculated for the S_0 and unrestricted T_1 states, with the B3LYP functional for all compounds, using the "polar" keyword. The Dunning-style cc-pVDZ basis set[48] was used for all G09 molecular calculations. An in-house program, which employs the numerical integration method of Becke and Dickson,[49] was used to calculate the H_{12} integrals.

III. RESULTS AND DISCUSSION

A. Replication of Piezochromism

Applying our computational scheme, we obtained the absorption/emission energies for each crystal under a series of pressure values. The pressure ranges considered for the four crystal structures are: FIFGUY01/FIFGUY02 (**1**): 0.0-4.0 GPa (in 0.5 GPa increments); XAPLUY (**2**): 0.0-6.0 GPa (in 0.5 GPa increments); IXICUP (**3**): 0-15 GPa (in 1 GPa increments). The emission energies as functions of pressure are presented in Figure 3, with comparison to the experimental emission data extracted from literature.[28–30] Similar results were also obtained for the absorption energies versus pressure, as shown in the Supplementary Information. For each molecular crystal, red shift of the emission from the absorption is predicted for the entire pressure range, in agreement with the experimental observations.

Overall, our calculations were able to replicate the piezochromism of the modeled molecular crystals. As Figure 3 shows, the calculated emission energies red shift with increased external pressure for all four molecular crystals, which is consistent with the experimentally observed trends. Note that the calculated "compression curves" for the excitation energies are smooth. This suggests a gradual and reversible red shift of the excitation energy as the external pressure is increased within the calculated range, which also agrees with experimental observations. We point out that the results for the two crystals of **1** (FIFGUY01 and FIFGUY02) are essentially identical, which indicates that the geometry optimizations correctly "linked" the two ends of the same reversible compression cycle.[28] Compression from the low-pressure structure and decompression from the high-pressure structure lead to identical piezochromic behavior; for this reason, we shall report only on FIFGUY01 in our further discussions.

In terms of eV-accuracy, our predictions over-estimate the experimental emission energies by *ca.* 0.40 eV for **1** and 0.25 eV for **2**, while an under-estimation by *ca.* 0.45 eV occurred for **3**. These errors are comparable to those previously obtained for three organic push-pull molecules (0.24-0.40 eV).[33] However, the relative changes in $\Delta E_{0S}^{\mathrm{emi}}$ with pressure are in more impressive agreement with experiment. As shown in Table II, the predicted magnitudes of the piezochromic red shifts and their pressure derivatives (*i.e.* the slopes of the emission compression curves) match very closely to the experimental data.

By decomposing our calculated singlet-excitation energies

FIG. 3: Calculated emission energies (ΔE_{0S}^{emi}) versus applied pressure, decomposed into the triplet-excitation (ΔE_{0T}^{emi}) and the H_{12}^{mol} integral contributions. The triplet excitation energies for the excised molecules (ΔE_{0T}^{mol}) are also shown. The calculated results are compared to experimentally-measured emission energies under varying pressure (ΔE_{0S}^{exp}). Panels (a-d) correspond to the results for FIFGUY01, FIFGUY02, XAPLUY, and IXICUP, respectively.

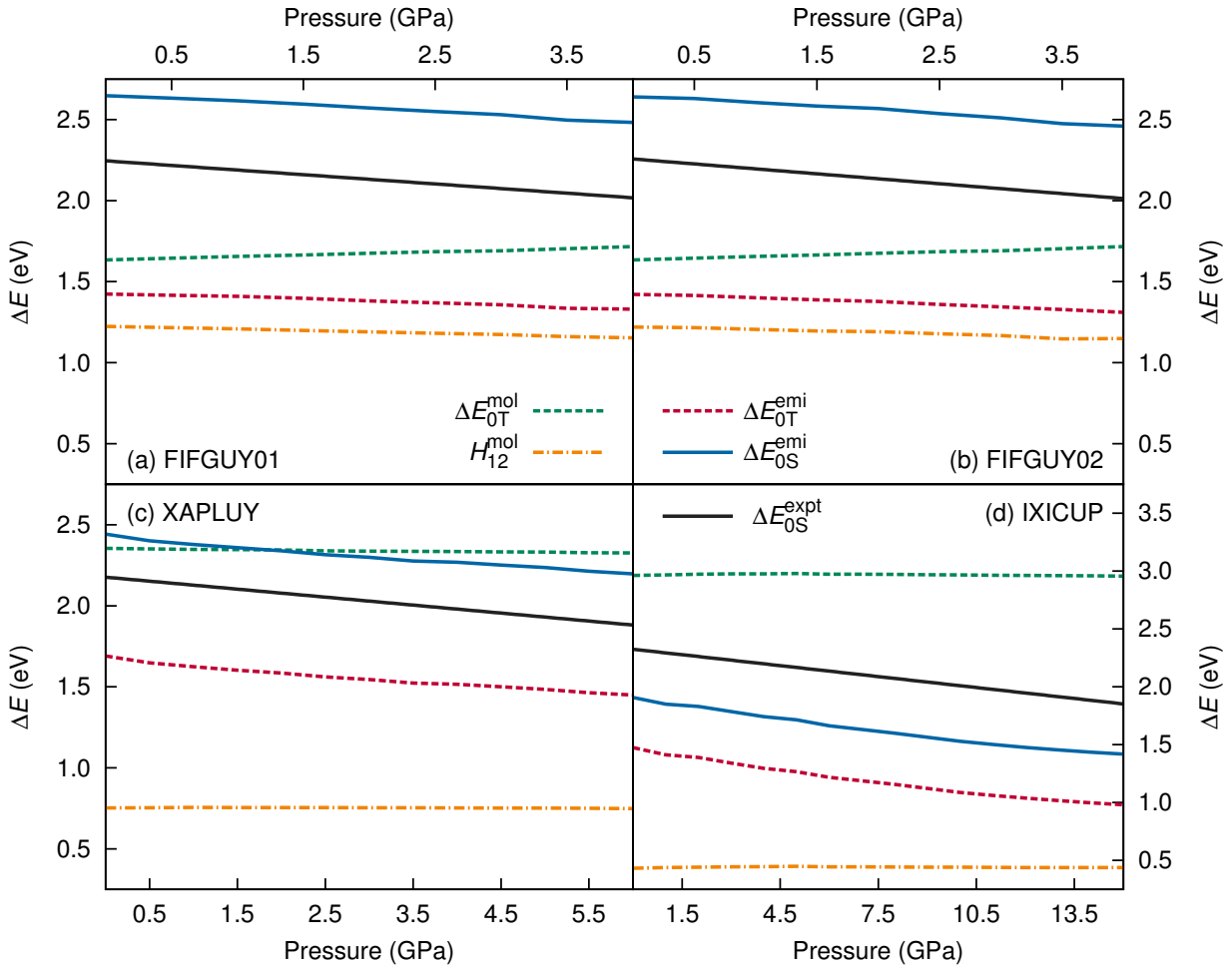

TABLE II: Calculated emission piezochromism, showing both the total red shift (eV) and red shift per unit pressure (eV/GPa). Results, linearly fit and interpolated to match the full experimental pressure ranges, are shown for both the full calculations of the S_1 excitation energy (ΔE_{0S}^{emi}) and the T_1 band gaps (ΔE_{T1}^{gap}). The band-structure calculations correspond to the difference between valence and conduction band edges from the ground-state electronic configuration, using the T_1 geometries for each applied pressure. Experimental data are given for comparison.

Species	Total red shift			Shift per unit pressure		
	ΔE_{0S}^{emi}	ΔE_{T1}^{gap}	Expt.	ΔE_{0S}^{emi}	ΔE_{T1}^{gap}	Expt.
1	0.14	0.13	0.19	0.044	0.041	0.059
2	0.22	0.27	0.26	0.038	0.047	0.045
3	0.48	0.52	0.53	0.033	0.036	0.037

into the triplet-excitation and H_{12} integral contributions, as in Figure 3, it can be argued that the piezochromism of the investigated molecular crystals is driven by pressure-induced changes in the intermolecular interactions. For each compound in Figure 3, the values of the H_{12} integrals and intramolecular triplet excitation energies are nearly constant with respect to pressure. Thus, the overall piezochromic red shift is determined primarily from the solid-state triplet excitation energy. These results indicate the importance of properly accounting for the non-covalent, intermolecular interactions within the crystal lattice when modeling piezochromism.

B. Origin of the Universal Red Shift

One intriguing observation from both the experimental and calculated excitation-energy data is the consistent finding of a red shift with increased isotropic pressure. The fact that this red-shift behavior is shared by most other reported piezochromic molecular crystals in the experimental literature implies the universality of its origin. We suggest that the

FIG. 4: Potential energy curves for the S_0 and S_1 states of the molecular crystals as functions of applied pressure. Panels (a-c) correspond to the results for FIFGUY01, XAPLUY, and IXICUP, respectively.

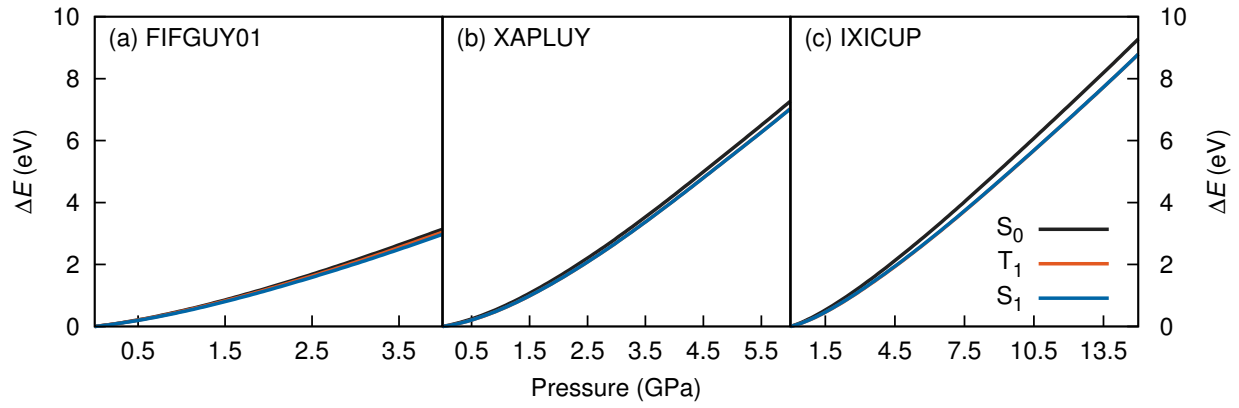

piezochromic red shift can be rationalized from two different perspectives: molecular and solid-state.

1. *The Molecular Polarizability Perspective*

From a molecular point of view, one might suspect that the piezochromic red shift could be caused by the difference in the response of the molecule in the ground or excited state to increasing pressure. The ground- and excited-state energies are each expected to increase with pressure due to confinement effects, as shown in Figure 4 (note that the S_1 curves are directly above the T_1 for XAPLUY and IXICUP). However, the energy of the ground state is raised to a larger degree than the excited states when the surrounding crystal lattice is compressed, reducing the excitation energy and leading to a pressure-induced red shift. This result can be explained if the excited-state molecule, which typically possesses a more diffuse electronic density than the ground state, is more able to polarize itself to adapt to increasing spacial constriction. Applied pressure increases Pauli repulsion between molecules. The densities of highly malleable (*i.e.* highly polarizable) molecules are better able to adjust themselves to avoid density overlaps and hence reduce Pauli repulsion. This reasoning is akin to a similar polarization argument made by Feng *et al.* in their experimental work.[12]

TABLE III: Molecular S_0 and T_1 polarizabilities (in a.u.) calculated for the excised molecules at zero pressure, using the crystal geometries obtained for either the absorption or emission.

Species	S_0 Polarizability		T_1 Polarizability	
	Abs.	Emi.	Abs.	Emi.
1	301	327	381	372
2	390	393	591	588
3	303	310	508	500

To validate the hypothesis of the excited states being more polarizable, we calculated the polarizabilities of the excised molecules in both S_0 and T_1 states. Results for both the zero-pressure absorption and emission geometries are summarized in Table III. At zero pressure, the polarizability of the excised molecular moiety is significantly higher for the T_1 state than for the S_0 state of each species. The same trend holds for the full pressure ranges as well, albeit both the S_0 and T_1 polarizabilities decline slightly at higher pressures (see Supplementary Information). Thus, for the investigated species, the single molecule becomes more polarizable in the excited state, which induces the piezochromic red shift of the excitation energy via reduction of intermolecular repulsion. However, there is no direct correlation between the T_1-S_0 polarizability difference and the red shift per unit pressure, which is expected as the extent of compression will be highly anisotropic, depending on the molecular packing.

2. *The Solid-State Band Structure Perspective*

Alternatively, when one considers the entire crystal lattice, it is also of potential value to probe the effect of increased pressure on the calculated band structure. We might reasonably expect that external pressure will change (even if only slightly) the band gap of the compressed crystal. The crystal band gap is directly linked to the first-singlet excitation energy and the behavior of a molecular crystal's band gap under pressure could indicate its piezochromism. We hence conducted standard ground-state band-structure calculations for the investigated molecular crystals over the entire range of applied pressures. In each case, up to 6 bands above the conduction band edge were calculated. The resulting bands are extremely flat, as expected for molecular systems; representative band structures are shown in the Supplementary Information.

Figure 5 shows the variation in the valence and conduction band edges, which correspond to the highest-occupied and lowest-unoccupied bands, computed at the T_1 (emission) optimized geometries. These individual band energies both increase with pressure, due to molecular confinement. The crystal band gap values were extracted from the calculated band structure and are also plotted in Figure 5. The band gaps

FIG. 5: Valence and conduction band edges, and band gaps, of the molecular crystals as functions of applied pressure, using the T_1 geometries. Panels (a-c) correspond to the results for FIFGUY01, XAPLUY, and IXICUP, respectively.

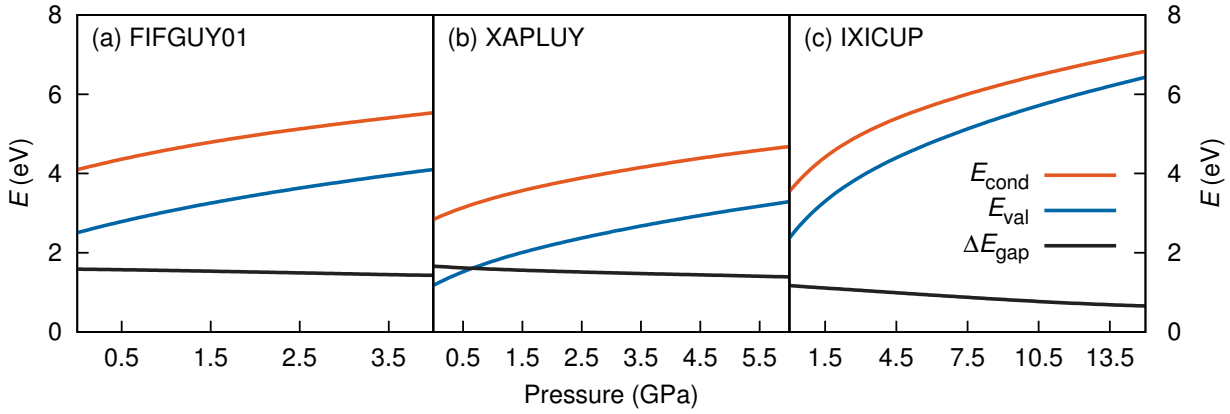

are consistently lower than the T_1 excitation energies obtained from the difference in self-consistent energies, as expected for the type of density-functional approximation used.[50–53] The band gaps for all three crystals smoothly decrease with pressure, in agreement with the observed piezochromism. The maximum emission red shifts are compared with the full computational results and the experimental data in Table II. The red shifts in the band gap and in the full S_1 excitation energy with pressure are virtually identical for all three molecular crystals. Thus, we can view the pressure-induced closing of the band gap as driving piezochromism.

IV. CONCLUSION

In this work, a novel computational scheme, combining solid-state and gas-phase DFT and Becke's virial exciton model, was proposed and applied to predict the piezochromism for a selection of molecular crystals. Our results indicate that the proposed method correctly captures the experimentally observed piezochromic red shifts. The magnitudes of the red shifts, and their rates of change with applied pressure, were predicted with impressive accuracy. Our calculations also revealed that the piezochromism observed for the investigated molecular crystals is predominantly a result of pressure modulation of the intermolecular interactions within the crystal lattice. Further, theoretical insights into the origin of the universal piezochromic red shift were gained. We found that the piezochromic red shift could be rationalized from two perspectives: i) molecular, as the polarizability of the excited moiety consistently increases upon excitation, preferentially stabilizing the excited state upon compression; and ii) solid state, as closing of the crystal band gap under increasing pressure is consistently predicted. We hope that this work will contribute to the understanding of piezochromism and electronic excitations in molecular crystals in general, and aid the design of novel molecular crystals displaying PL properties of potential applicability.

SUPPLEMENTARY MATERIAL

Calculated absorption energies as functions of pressure; molecular polarizabilities for the S_0 and T_1 states as functions of pressure; valence and conduction band edges and band gaps as functions of pressure using the solid-state S_0 geometries; representative zero-pressure band structures.

DATA AVAILABILITY STATEMENT

The data that support the findings of this study are available from the corresponding author upon reasonable request.

ACKNOWLEDGMENTS

E.R.J. and A.D.B. thank the Natural Sciences and Engineering Research Council of Canada (NSERC), and F.X. acknowledges the Government of Nova Scotia for financial support. The authors thank Compute Canada for providing computational resources.

[1] Y. Sagara and T. Kato, Nature Chemistry **1**, 605 (2009).
[2] Z. Ning, Z. Chen, Q. Zhang, Y. Yan, S. Qian, Y. Cao, and H. Tian, Adv. Funct. Mater. **17**, 3799 (2007).
[3] Y. Sagara, S. Yamane, M. Mitani, C. Weder, and T. Kato, Adv. Mater. **28**, 1073 (2016).
[4] Z. Chi, X. Zhang, B. Xu, X. Zhou, C. Ma, Y. Zhang, S. Liu, and J. Xu, Chem. Soc. Rev. **41**, 3878 (2012).
[5] S. Hirata and T. Watanabe, Adv. Mater. **18**, 2725 (2006).
[6] Y. Ooyama, T. Okamoto, T. Yamaguchi, T. Suzuki, A. Hayashi, and K. Yoshida, Chem. Eur. J. **12**, 7627 (2006).
[7] W. C. H. Choy, W. K. Chan, and Y. Yuan, Adv. Mater. **26**, 5368 (2014).
[8] J. Luo, Z. Xie, J. W. Y. Lam, L. Cheng, H. Chen, C. Qiu, H. S. Kwok, X. Zhan, Y. Liu, D. Zhu, and B. Z. Tang, Chem. Commun. , 1740 (2001).
[9] J. Mei, N. L. C. Leung, R. T. K. Kwok, J. W. Y. Lam, and B. Z. Tang, Chem. Rev. **115**, 11718 (2015).
[10] M. Sase, S. Yamaguchi, Y. Sagara, I. Yoshikawa, T. Mutai, and K. Araki, J. Mater. Chem. **21**, 8347 (2011).
[11] Y. Dong, J. Zhang, X. Tan, L. Wang, J. Chen, B. Li, L. Ye, B. Xu, B. Zou, and W. Tian, J. Mater. Chem. C **1**, 7554 (2013).
[12] C. Feng, K. Wang, Y. Xu, L. Liu, B. Zou, and P. Lu, Chem. Commun. **52**, 3836 (2016).

[13]M. Yoshida, F. Nakanishi, T. Seki, K. Sakamoto, and H. Sakurai, Macromolecules **30**, 1860 (1997).
[14]E. L. Harty, A. R. Ha, M. R. Warren, A. L. Thompson, D. R. Allan, A. L. Goodwina, and N. P. Funnell, Chem. Commun. **51**, 10608 (2015).
[15]Q. Qi, J. Qian, X. Tan, J. Zhang, L. Wang, B. Xu, B. Zou, and W. Tian, Adv. Funct. Mater. **25**, 4005 (2015).
[16]Y. Liu, Q. Zeng, B. Zou, Y. Liu, B. Xu, and W. Tian, Angew. Chem. Int. Ed. **57**, 15670 (2018).
[17]T. Zhang, W. Shi, D. Wang, S. Zhuo, Q. Peng, and Z. Shuai, J. Mat. Chem. C **7**, 1388–1398 (2019).
[18]E. Runge and E. K. U. Gross, Phys. Rev. Lett. **52**, 997 (1984).
[19]M. Petersilka, U. J. Gossmann, and E. K. U. Gross, Phys. Rev. Lett. **76**, 1212 (1996).
[20]A. Warshel and M. Levitt, J. Mol. Biol. **103**, 227 (1976).
[21]Y. Jin, E. R. Johnson, X. Hu, W. Yang, and H. Hu, J. Comput. Chem. **34**, 2380 (2013).
[22]C. M. Isborn, B. D. Mar, B. F. E. Curchod, I. Tavernelli, and T. Martínez, J. Phys. Chem. B **117**, 12189 (2013).
[23]J. R. G. Sander, D. Bučar, R. F. Henry, J. Baltrusaitis, G. G. Z. Zhang, and L. R. MacGillivray, J. Pharm. Sci. **99**, 3676 (2010).
[24]M. Arhangelskis, M. D. Eddleston, D. G. Reid, G. M. Day, D. Bučar, A. J. Morris, and W. Jones, Chem. - Eur. J. **22**, 10065 (2016).
[25]M. Arhangelskis, D. B. Jochym, L. Bernasconi, T. Friščić, A. J. Morris, and W. Jones, J. Phys. Chem. A **122**, 7514 (2018).
[26]J. Hutter, J. Chem. Phys. **118**, 3928 (2003).
[27]C. R. Groom, I. J. Bruno, M. P. Lightfoot, and S. C. Ward, Acta Cryst. **B72**, 171 (2016).
[28]K. Nagura, S. Saito, H. Yusa, H. Yamawaki, H. Fujihisa, H. Sato, Y. Shimoikeda, and S. Yamaguchi, J. Am. Chem. Soc. **135**, 10322 (2013).
[29]L. Wang, K. Wang, B. Zou, K. Ye, H. Zhang, and Y. Wang, Adv. Mater. **27**, 2918 (2015).
[30]J. Wu, Y. Cheng, J. Lan, D. Wu, S. Qian, L. Yan, Z. He, X. Li, K. Wang, B. Zou, and J. You, J. Am. Chem. Soc. **138**, 12803 (2016).
[31]P. E. Blöchl, Phys. Rev. B **50**, 17953 (1994).
[32]A. D. Becke, J. Chem. Phys. **148**, 044112 (2018).
[33]X. Feng, A. D. Becke, and E. R. Johnson, J. Chem. Phys. **149**, 231101 (2018).
[34]X. Feng, A. Otero-de-la-Roza, and E. R. Johnson, Can. J. Chem. **96**, 730–737 (2018).
[35]A. Otero-de-la-Roza, E. R. Johnson, and V. Luaña, Comput. Phys. Commun. **185**, 1007–1018 (2014).
[36]The postg program is available from http://schooner.chem.dal.ca.
[37]A. D. Becke, J. Chem. Phys. **86**, 7184 (1986).
[38]J. P. Perdew, K. Burke, and M. Ernzerhof, Phys. Rev. Lett. **78**, 1396 (1996).
[39]A. D. Becke and E. R. Johnson, J. Chem. Phys. **127**, 154108 (2007).
[40]A. D. Becke and E. R. Johnson, J. Chem. Phys. **127**, 124108 (2007).
[41]A. Otero-de-la-Roza and E. R. Johnson, J. Chem. Phys. **136**, 2012 (2012).
[42]P. Giannozzi, O. Andreussi, T. Brumme, O. Bunau, M. B. Nardelli, M. Calandra, R. Car, C. Cavazzoni, D. Ceresoli, M. Cococcioni, N. Colonna, I. Carnimeo, A. D. Corso, S. de Gironcoli, P. Delugas, R. A. DiStasio, A. Ferretti, Jr., A. Floris, G. Fratesi, G. Fugallo, R. Gebauer, U. Gerstmann, F. Giustino, T. Gorni, J. Jia, M. Kawamura, H. Ko, A. Kokalj, E. Küçükbenli, M. Lazzeri, M. Marsili, N. Marzari, F. Mauri, N. L. Nguyen, H. Nguyen, A. Otero-de-la-Roza, L. Paulatto, S. Poncé, D. Rocca, R. Sabatini, B. Santra, M. Schlipf, A. P. Seitsonen, A. Smogunov, I. Timrov, T. Thonhauser, P. Umari, N. Vast, X. Wu, and S. Baroni, J. Phys.: Condens. Matter **29**, 465901 (2017).
[43]H. J. Monkhorst and J. D. Pack, Phys. Rev. B **13**, 5188 (1976).
[44]A. Dal Corso, Comput. Mater. Sci. **95**, 337 (2014).
[45]A. D. Becke, J. Chem. Phys. **98**, 5648 (1993).
[46]A. D. Becke, J. Chem. Phys. **98**, 1372 (1993).
[47]M. J. Frisch, G. W. Trucks, H. B. Schlegel, G. E. Scuseria, M. A. Robb, J. R. Cheeseman, G. Scalmani, V. Barone, B. Mennucci, G. A. Petersson, H. Nakatsuji, M. Caricato, X. Li, H. P. Hratchian, A. F. Izmaylov, J. Bloino, G. Zheng, J. L. Sonnenberg, M. Hada, M. Ehara, K. Toyota, R. Fukuda, J. Hasegawa, M. Ishida, T. Nakajima, Y. Honda, O. Kitao, H. Nakai, T. Vreven, J. A. Montgomery, Jr., J. E. Peralta, F. Ogliaro, M. Bearpark, J. J. Heyd, E. Brothers, K. N. Kudin, V. N. Staroverov, R. Kobayashi, J. Normand, K. Raghavachari, A. Rendell, J. C. Burant, S. S. Iyengar, J. Tomasi, M. Cossi, N. Rega, J. M. Millam, M. Klene, J. E. Knox, J. B. Cross, V. Bakken, C. Adamo, J. Jaramillo, R. Gomperts, R. E. Stratmann, O. Yazyev, A. J. Austin, R. Cammi, C. Pomelli, J. W. Ochterski, R. L. Martin, K. Morokuma, V. G. Zakrzewski, G. A. Voth, P. Salvador, J. J. Dannenberg, S. Dapprich, A. D. Daniels, Ö. Farkas, J. B. Foresman, J. V. Ortiz, J. Cioslowski, and D. J. Fox, "Gaussian 09 Revision E.01," Gaussian Inc. Wallingford CT 2009.
[48]T. H. Dunning, Jr., J. Chem. Phys. **90**, 1007 (1989).
[49]A. D. Becke and R. M. Dickson, J. Chem. Phys. **89**, 2993 (1988).
[50]A. Seidl, A. Görling, P. Vogl, J. Majewski, and M. Levy, Phys. Rev. B **53**, 3764 (1996).
[51]P. Mori-Sánchez, A. J. Cohen, and W. Yang, Phys. Rev. Lett. **100**, 146401 (2008).
[52]S. Refaely-Abramson, R. Baer, and L. Kronik, Phys. Rev. B **84**, 075144 (2011).
[53]E. Kraisler and L. Kronik, J. Chem. Phys. **140**, 18A540 (2014).